Effect of Joule heating on current-induced asymmetries and breakdown of the quantum Hall effect in narrow Hall bars

Rolf R. Gerhardts

Max-Planck-Institut für Festkörperforschung, Heisenbergstrasse 1, D-70569 Stuttgart, Germany

HIGHLIGHTS

- Joule heating is incorporated into a self-consistent theory of screening and magneto-transport in narrow Hall bars.
- Current-induced asymmetries of the current distribution are calculated under the conditions of the integer-quantized Hall effect and its breakdown.
- Comparison with recent experiments shows that the present calculations, assuming a simplified sample geometry, can nicely explain some of the breakdown results, whereas others seem to result from spatial inhomogeneities.

ARTICLE INFO

ABSTRACT

Recent low-temperature scanning-force-microscopy experiments on narrow Hall bars, under the conditions of the integer quantum Hall effect (IQHE) and its breakdown, have revealed an interesting position dependence of the Hall potential, which changes drastically with the applied magnetic field and the strength of the imposed current through the sample. The present paper shows, that inclusion of Joule heating into an existing self-consistent theory of screening and magneto-transport, which assumes translation invariant Hall bars with a homogeneous background charge due to doping, can explain the experimental results on the breakdown of the IQHE in the so called edge-dominated regime.

© 2016 The Authors. Published by Elsevier B.V. This is an open access article under the CC BY-NC-ND license (http://creativecommons.org/licenses/by-nc-nd/4.0/).

1. Introduction

The interplay of low-temperature scanning-force-microscopy (SFM) experiments [1–5] and a self-consistent theory of screening and magneto-transport [6–9], based on a local-equilibrium description of the stationary, current-carrying non-equilibrium states, has led to a good understanding and consistent description of the integer-quantized Hall effect (IQHE) [10] in narrow Hall bars (width ~10 μm). Early experiments [3] showed that, for perpendicular magnetic fields B in the low-B regime of a quantized Hall plateau (QHP), the imposed current flows through two stripes near the opposite edges of the sample, so that the resulting Hall potential increases step-like across these stripes and is constant in between. From the B-dependence of the position of these stripes they could be identified as the "incompressible stripes" (ISs) [11,12], which exist as a consequence of the non-linear screening properties of the two-dimensional electron system (2DES) in strong magnetic fields at low temperatures [13,14].

A combination of this self-consistent screening theory with a simple transport theory, based on a local version of Ohm's law with a position-dependent conductivity tensor and the gradient of the electro-chemical potential as driving electric field, could explain these experiments and, at least qualitatively, the different current and Hall potential distributions for other magnetic field regimes [6]. These self-consistent calculations produced, as a non-linear feedback effect, a pronounced current-induced asymmetry of the ISs, which however had not clearly been seen in the early experiments [3]. But recent experiments, which used suitable unidirectional current pulses, could clearly confirm this current-induced asymmetry [5,15]. The theoretically predicted asymmetry was clearly seen in the "edge-dominated" regime, in which the imposed current flows through ISs near the sample edges and the B-field has values near the low-B edges of a QHP. These results differ substantially from those obtained in the "bulk-dominated" region, where the B-field resides in the high-B part of the QHP, and the density of the imposed current and the resulting Hall potential vary over a wide part of the bulk of the sample.

Motivated by these new experimental results, the self-consistent screening and magneto-transport theory was applied to investigate in some detail the dependence of the spatial distribution of the imposed current and the resulting Hall potential on different parameters, such as magnetic field, temperature, collision-broadening of Landau levels, and strength of the imposed current [9].

E-mail address: R.Gerhardts@fkf.mpg.de

The results were not in all aspects in agreement with the experiments. Fig. 6 of [9] shows, for example, that with increasing strength of the imposed current the asymmetry increases and eventually nearly all current flows through one of the ISs, while the bulk is free of current. In the experiment, on the other hand, a similar behavior is seen for small imposed currents, but for larger currents an increasing part of the imposed current flows through the dissipative bulk, so that a continuous breakdown of the IQHE is observed. To overcome this discrepancy, apparently a breakdown mechanism must be considered in the calculation. In the following we will include in the previously used self-consistent theory of screening and magneto-transport the effect of local Joule heating, which has been discussed in the literature as the most relevant mechanism for the breakdown of the IQHE [16–18]. We will see, that the importance of Joule heating depends strongly on temperature and the strength of the imposed current, and that the calculations yield reasonable agreement with experimental results in the edge-dominated regime. In the bulk-dominated regime, where the experiments indicate the importance of long-range density fluctuations, the present model of a laterally confined translation invariant 2DES with a homogeneous background of doping charges seems not to be sufficient.

2. Model

We keep our model as close as possible to that used in previous work [6,8,9]. In particular, we assume that all charges, i.e. donor charges, the 2DES, and the induced charges on the in-plane metal gates, are in the plane $z=0$. Further we assume translation invariance in y-direction and lateral confinement of donor density $n_D(x)$ and electron density $n_{el}(x)$ to the interval $|x| < d$ by the in-plane metal gates at $|x| > d$. We neglect exchange and correlation effects in the 2DES, as well as spin splitting, and we replace the mutual interaction of an electron with the other electrons by its interaction with an effective Hartree potential generated by the total electron density. These assumptions allow an exact evaluation of the electrostatic potential $V(x, z)$ [11,12] with $V(x, 0) = V_D(x, 0) + V_G(x) + V_H(x, 0)$, where

$$V_D(x, 0) + V_H(x, 0) = -\frac{2e^2}{\bar{\kappa}} \int_{-d}^{d} dx' K(x, x')[n_D(x') - n_{el}(x')], \quad (1)$$

with the kernel

$$K(x, x') = \ln\left|\left[\sqrt{(d^2 - x^2)(d^2 - x'^2)} + d^2 - x'x\right] \Big/ \left[(x - x')d\right]\right|, \quad (2)$$

is the sum of the confinement potential due to the donors, $V_D(x, 0)$, and the Hartree potential $V_H(x, 0)$, respectively. With constant gate potentials $V(x, 0) = V_L$ for $x < -d$ and $V(x, 0) = V_R$ for $x > d$ one obtains $V_G(x) = (V_L + V_R)/2 + (V_R - V_L)\arcsin(x/d)/\pi$ for the potential generated by the gates. The above assumptions allow also to calculate the induced charges on the gates [6]. In the following we will consider source-drain currents flowing through the sample under "floating gate conditions", which do not allow for a charge transfer between the two gates. These conditions can be realized [6] by fixing the quantity

$$Q_R = -(2e/\pi) \int_{-d}^{d} dx[n_D - n_{el}(x)]\arctan\sqrt{(d + x)/(d - x)}. \quad (3)$$

As in previous work, we consider only a constant donor charge density en_D, which leads to the potential $V_D(x, 0) = -E_D[1 - (x/d)^2]^{1/2}$, with $E_D = 2\pi e^2 n_D d/\bar{\kappa}$, and leave the consideration of a modulated $n_D(x)$ for later work.

A fundamental approximation of our approach is, that the effective electrostatic potential energy $V(x) \equiv V(x, z = 0)$ varies

within the 2DES slowly on the scale of the magnetic length $\ell_B = \sqrt{\hbar c/eB}$, which defines the spatial extent of Landau wavefunctions, and on the scale of the Fermi wavelength, which is of the order of the average distance between electrons in the 2DES. Then the Hartree approximation reduces to the Thomas-Fermi approximation [8,9] and the electron density in Eq. (1) can be written as

$$n_{el}(x) = \int dE \, D(E)f([E + V(x) - \mu^\star]/k_BT), \quad (4)$$

where $D(E)$ is the density of states of a homogeneous 2DES in the same constant magnetic field without the energy $V(x)$ and $f(\varepsilon) = 1/[1 + \exp(\varepsilon)]$ denotes the Fermi function. In thermal equilibrium, i.e., without imposed current, the electrochemical potential $\mu^\star$ and the temperature T are constant, and $V(x)$ and $n_{el}(x)$ have to be calculated self-consistently from Eqs. (1) and (4), which define in general a non-linear integral equation for the effective confinement potential $V(x)$. In the absence of magnetic fields $(B=0)$, $D(E)$ for the 2DES in GaAs can be taken as constant, $D(E) = D_0\theta(E)$ with $D_0 = m/(\pi\hbar^2) = 2.79 \times 10^{10}/(\text{meV cm}^2)$, so that for $T=0$ this integral equation becomes linear in $V(x)$ for $-d < x_{min} \leq x \leq x_{max} < d$ with $V(x_{min}) = V(x_{max}) = \mu^\star$ and is easily solved numerically.

As in previous work [9] we assume in the following a homogeneous background charge density en_D, with $n_D = 4 \cdot 10^{11} \text{ cm}^{-2}$, and a sample-width $2d = 3 \, \mu\text{m}$. Requiring that, for $B=0$ and $T=0$, the electron density $n_{el}(x)$ vanishes for $|x| > 0.9d$, we obtain an average electron density $\langle n_{el} \rangle = (2d)^{-1} \int_{-d}^{d} dx \, n_{el}(x) = 2.9 \cdot 10^{11} \text{ cm}^{-2}$, which we keep fixed. This model leads to a density profile $n_{el}(x)$ that decreases monotonically from its maximum in the center to the depleted stripes near the edges of the Hall bar. As a consequence, for a given B-value at most two ISs with the same integer filling factor, e.g. $\nu(x) = 2$, are possible.

As in [6,9] we describe a *stationary non-equilibrium state* with an imposed current I along the Hall bar, assuming *local equilibrium* with a position-dependent electrochemical potential $\mu^\star(x)$ in Eq. (4), where the position-dependence follows from the local form of Ohm's law, $\mathbf{j}(\mathbf{r}) = \hat{\sigma}(\mathbf{r})\mathbf{E}(\mathbf{r})$, with the gradient of the electrochemical potential $\mu^\star(\mathbf{r})$ as driving electric field, $\mathbf{E} = \nabla \mu^\star/e$. Explicit expressions for the position-dependent conductivity components and the resulting current densities and electric fields are given in [9] and collected in the Appendix. In a stationary state of the sample with the properties mentioned before, the components $E_y(x) = E_y^0$ and $j_x(x) = j_x^0$ must be constant, and, due to the depletion stripes between the 2DES and the gates, the current across the sample vanishes, $j_x(x) \equiv 0$.

In addition to the treatment of [9], we now consider Joule heating $W(x) = E_y^0 j_y(x)$. In a stationary state of the 2DES the produced heat must be transferred to the surrounding lattice. To keep things simple, we neglect the possibility of heat flow within the 2DES and assume that only the direct local heat transfer $P_L(x)$ to the lattice is important. This will depend on the difference between local electron temperature $T_{el}(x)$ and lattice temperature T_L. Assuming that this difference is sufficiently small, we take from the literature [19] the linearized form $P_L(x) = C_p^0 D_T(x)(T_{el}(x) - T_L)$, where C_p^0 describes the effect of electron-phonon scattering and $D_T(x) = \partial n_{el}(x)/\partial \mu^\star(x)$ denotes the thermodynamic density of states at position x. The balance of Joule heating and heat transfer to the lattice then yields for the local electron temperature

$$T_{el}(x) = T_L + \Delta T(x), \quad \Delta T(x) = (2p/C_p^0)E_y^0 j_y(x)/D_T(x), \quad (5)$$

where we use $C_p^0 = (k_B/\hbar)10^{-3}(\text{meV})^2$ and introduce a parameter p to investigate different couplings to the lattice ($p=0.5$ corresponds to [19] and $p=0$ neglects Joule heating effects).

3. Results

3.1. Current-driven breakdown

As already mentioned in the introduction, in the edge-dominated regime there is a discrepancy between experiment and the calculation of [9], which neglected Joule heating, concerning the increase of the asymmetry of the ISs with increasing strength of the imposed current. Comparison of Figs. 1 and 2 shows that the consideration of Joule heating eliminates this discrepancy.

Fig. 1 recalls, for a typical case, the results without Joule heating as shown in Fig. 6 of [9] and, in addition, contains the linear response result. Here we choose equidistant mesh points x_n for $n = 0, 1, …, N$ with $N=700$ and calculate, as described in [9], for the collision broadening with $\gamma = 0.1$, the equilibrium state at $B=7$ T and $T=4$ K, and keep $\langle n_{el} \rangle$ and the induced charges on each gate fixed. This yields reasonably well developed incompressible stripes centered near $x = \pm 0.525d$. Then we apply a step-wise increasing current I, which modifies electro-chemical potential and, as a consequence, electron density and effective confinement potential, and we achieve self-consistency for each step. The upper panels of Fig. 1 show, near the ISs, for the linear response limit ($I \to 0$) and for four finite values of the applied current I, the resulting current density $j_y(x)$ (in units of the average current density $I/2d$) and the Landau level filling factor $\nu(x)$. The current density is confined to the ISs and with increasing I the IS centered near $x = 0.525d$, in which the applied current has the same direction as the intrinsic equilibrium current, becomes wider and carries nearly all the current, essentially without dissipation. The lower panel of Fig. 1 shows the resulting asymmetry of the normalized Hall potential. This result is similar to the experimental one for small I, but not for larger values of I.

If we consider Joule heating, as in Fig. 2 for $p=0.1$, the current-induced asymmetry is less pronounced, and for larger strength of the imposed current an increasing part of this current spreads out

from the ISs into the dissipative bulk, leading to the breakdown of the QHE. This is similar to the experimental finding. For $p=0.1$ this happens for $I \lesssim 1$ μA, as shown in Fig. 2: there exist no longer incompressible stripes with constant filling factor $\nu(x) \equiv 2$, and the Hall potential takes on a finite slope in the bulk. If we reduce the coupling to the lattice and take $p=0.5$, Joule heating becomes more effective and the breakdown sets in already for $I < 0.5$ μA.

The lower panels of Fig. 3, which show the resistances of the Hall bar (referring to a square of side-length $2d$) as functions of the imposed current, demonstrate the crucial effect of Joule heating. Without Joule heating ($p=0$) the applied current drives the resistances towards the quantized values $R_{Hall} = h/(2e^2)$ and $R_{long} = 0$, in agreement with the fact that the most relevant incompressible stripe becomes wider with increasing I, see Fig. 1. On the other hand, Joule heating drives the resistances away from the quantized values and works towards a continuous breakdown of the QHE, similar to that seen in the experiment [5]. It may be interesting to note that the deviation of the Hall resistance from the quantized value, $R_{Hall} - h/(2e^2)$, shows a very similar dependence on the applied current I as the longitudinal resistance R_{long}, although it is about an order of magnitude smaller.

The upper and medium panels of Fig. 3 show, in linear and logarithmic scales, respectively, the position-dependent increase of the electron temperature $T_{el}(x)$ over the constant lattice temperature $T_L = 4$ K. We consider again two cases for the strength of the heat transfer to the lattice. If this is quite effective, $p=0.1$, Joule heating is not very effective for $I \lesssim 0.5$ μA and yields an increase of $T_{el}(x)$ over T_L of about 1 K or less in the ISs and of less than about 10^{-6}K in the bulk region. These values increase to about 3 K in the ISs and 10^{-3}K in the bulk for the breakdown currents of about 1 μA. For $p=0.5$ Joule heating is considerably more effective and the breakdown values are already reached for $I \sim 0.5$ μA.
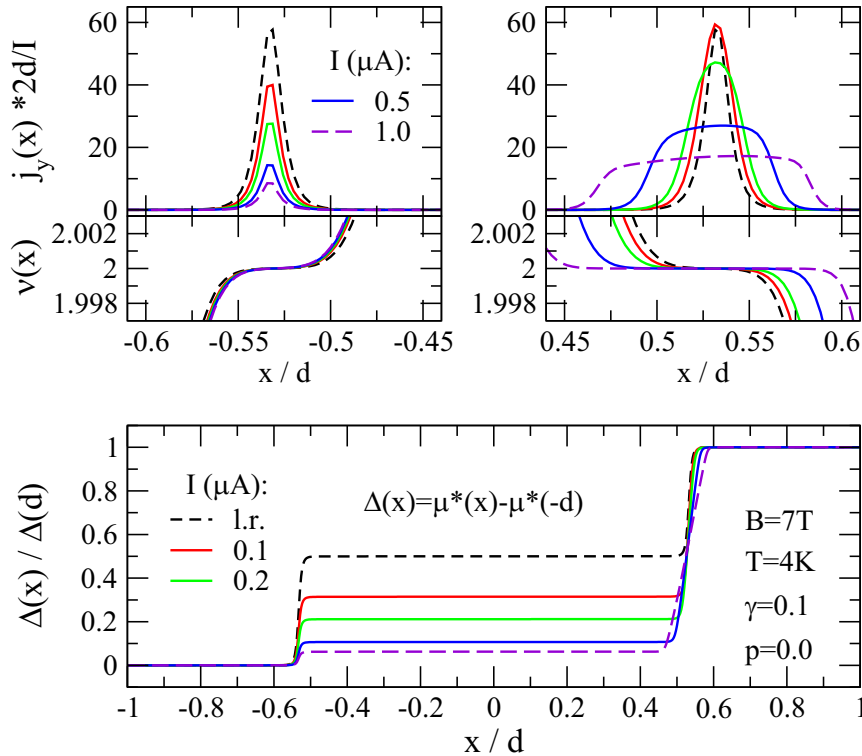

Fig. 1. Lower panel: normalized Hall potential; upper panels: current density $j_y(x)$ and filling factor $\nu(x)$, without Joule heating, $p=0$. The broken black lines show the linear response result; $N=700$, $\lambda = \ell_B$.
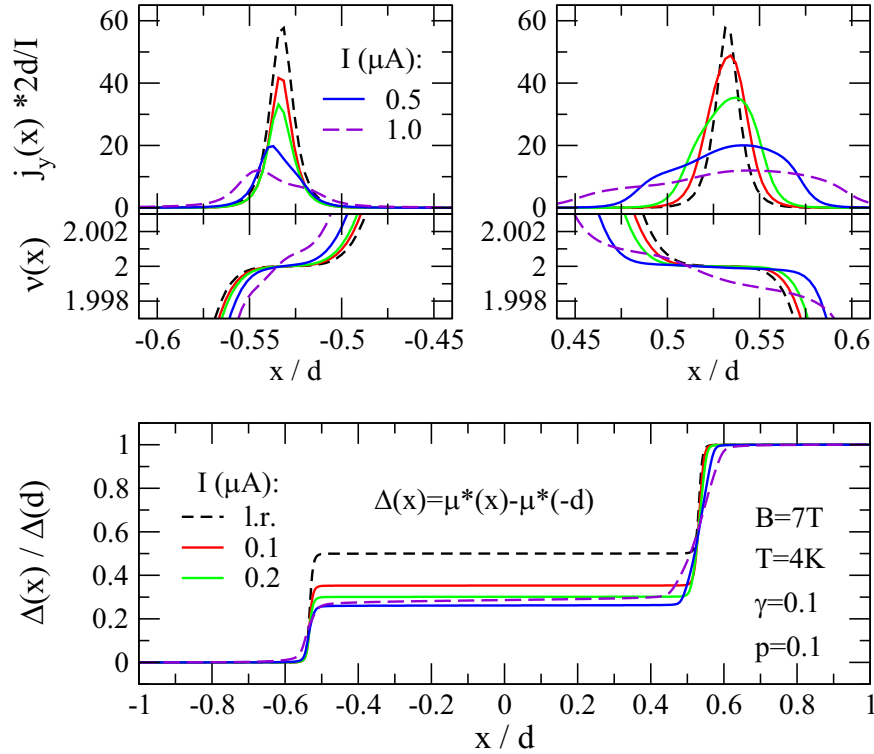
Fig. 2. Lower panel: normalized Hall potential; upper panels: $j_y(x)$ and $\nu(x)$ as in Fig. 1, but with consideration of Joule heating, $p=0.1$.

3.2. Temperature dependence

The results of the previous Section 3.1 indicate that, in the edge-dominated regime, simple Joule heating may be responsible for the breakdown of the QH effect. Comparing these results, which are calculated for a lattice temperature $T_L = 4$ K, with the experiments, which are presented in [5,9] and are taken at $T_L = 1.5$ K, we should however be careful, because the calculated resistances exhibit an intriguing temperature dependence. Typical results are presented in Fig. 4, which compares the situations with and without Joule heating. At high temperatures, $T_L \gtrsim 10$ K, the resistance is essentially independent of the imposed current (linear response regime). At lower temperatures the longitudinal resistivity decreases near the lines with local filling factor $\nu(x) = 2$, so that, according to the principle of minimal entropy production, the density of the imposed current develops maxima along these lines, so that R_{long} and the total dissipation decrease with decreasing T_L.

Without Joule heating ($p=0$, upper panels in Fig. 4) the main effect of the imposed current is to broaden the stripe in which most of the imposed current flows with low dissipation. Thus, at fixed $T_L \lesssim 4$ K the longitudinal resistance decreases with increasing imposed current, and no current-induced breakdown of the IQHE can be expected, see lower panels of Fig. 3.

Joule heating changes the situation drastically, as is shown in the lower panels of Fig. 4 for $p=0.1$. For $T_L \gtrsim 2.9$ K (i.e. K/$T_L \lesssim 0.36$) Joule heating increases the local electron temperature in the current-carrying region and thus leads, at fixed T_L, to an increase of R_{long} with increasing I, i.e. to the behavior we found in the lower panels of Fig. 3: with increasing I the resistances increase. For $T_L \lesssim 5$ K and low current (see the linear response result) R_{long} is about four orders of magnitude smaller than R_{Hall}, which is close to the quantized value $h/2e^2$. In the temperature range 3 K $\lesssim T_L \lesssim 5$ K increasing current I drives these resistances to higher values and so produces a continuous breakdown of the QH effect.

Near $T_L = 2.8$ K the situation becomes different. As I increases towards 1.5 μA, the slopes of the curves R_{long} versus $1/T_L$ become very steep, and for $I > 1.5$ μA these curves become discontinuous at a temperature $T_L = T_{\text{cr}}(I)$, which decreases with increasing I. The calculations for the solid curves in Fig. 4 start with $T_L = 50$ K and lower the temperature stepwise, keeping the imposed current fixed. If this current is sufficiently strong (here $I > 1.5$ μA), the system remains in a normal state with relatively large longitudinal resistance until the critical temperature $T_{\text{cr}}(I)$ is reached. As T_L is lowered further, we find at $T_L = T_{\text{cr}}(I)$ an abrupt transition to a state showing the IQHE. For $T_L < T_{\text{cr}}(I)$, R_{long} and $R_{\text{Hall}} - h/(2e^2)$ are many orders of magnitude smaller than h/e^2 and decrease further with decreasing T_L. This abrupt "phase transition" introduces a hysteretic behavior: if we lower T_L below $T_{\text{cr}}(I)$ and then increase T_L again, keeping I fixed, the system stays in a QH state for a temperature interval with $T_L > T_{\text{cr}}(I)$, until it jumps back to the unquantized, dissipative state at a higher temperature $T_L = T_{\text{cr}}^{\text{up}}(I) > T_{\text{cr}}(I)$, as is indicated in Fig. 4 by the broken lines. Characteristics of states in and close to such a hysteresis region are shown in Fig. 5 for the imposed current $I = 2$ μA with $T_{\text{cr}}(I) \approx 2.0417$ K $< T_{\text{cr}}^{\text{up}}(I) \approx 2.5833$ K. Outside the interval $T_{\text{cr}}(I) < T_L < T_{\text{cr}}^{\text{up}}(I)$ lowering and increasing T_L leads to the same state. In the QH states the density of the imposed current is strictly confined to the ISs, where R_{long} is extremely small so that heating is negligible. In the other states we observe broader current peaks around the lines with $\nu(x) = 2$, leading to an increase of the electron temperature by up to 8 K and the loss of ISs of finite width.

In the low-temperature region, where hysteretic behavior exists, we expect from Fig. 4 that, for a fixed $T_L < T_{\text{hys}} \approx 2.8$ K at low imposed currents I the system is in a QH state and the longitudinal resistance R_{long} decreases with increasing I (i.e. Joule heating is ineffective) until a critical current $I_{\text{cr}}(T_L)$ is reached, at which R_{long} suddenly increases by several orders of magnitude and the QH state breaks down. Depending on sample preparation and history, this transition will take place at a current I in the interval $I_1 \leq I \leq I_2$ defined by $T_{\text{cr}}(I_1) = T_L$ and $T_{\text{cr}}^{\text{up}}(I_2) = T_L$, since in this interval QH states and dissipative normal states coexist.

Fig. 4 is calculated for $p=0.1$ and without spatial averaging of
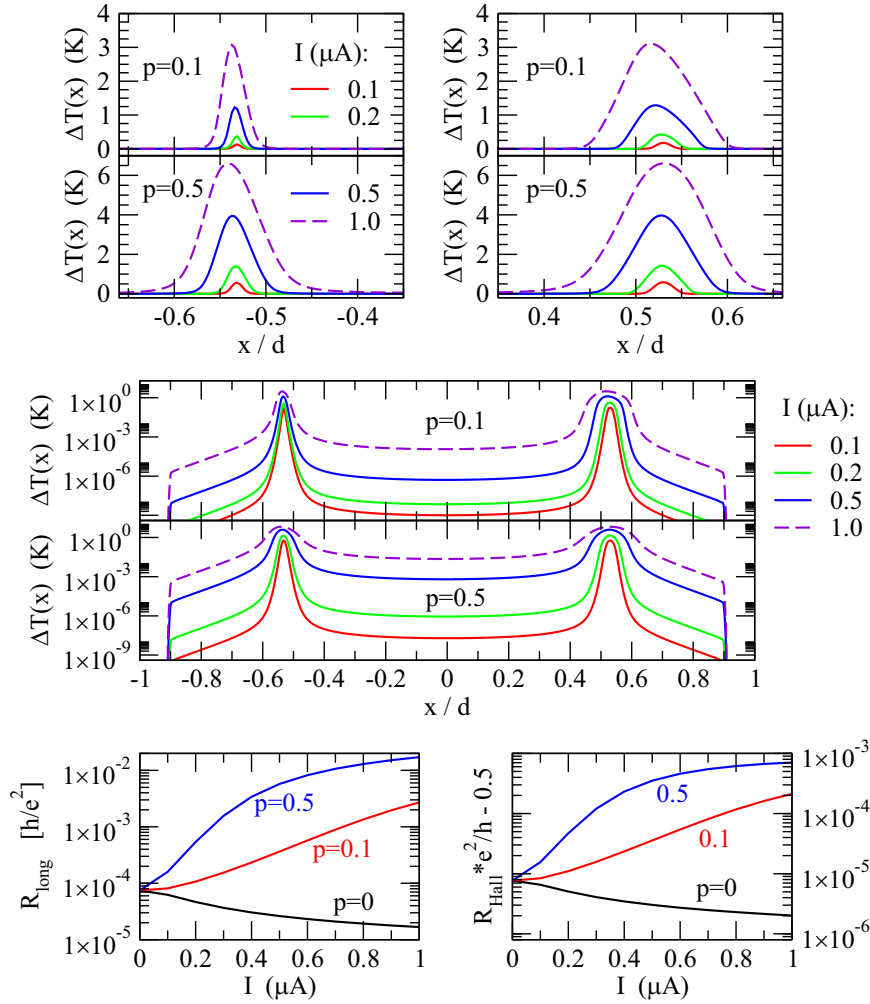
Fig. 3. Lower panels: longitudinal resistance $R_{long} = 2d\,E_y^0/I$ and Hall resistance $R_{Hall} = [\mu^\star(d) - \mu^\star(-d)]/(eI)$ versus applied current I without ($p=0$) and with ($p=0.1$ and $p=0.5$) Joule heating. Upper panels: Increase of electron temperature, $\Delta T(x) = T_{el}(x) - T_L$, due to Joule heating (for $p=0.1$ and $p=0.5$) for the indicated values of the applied current I. Medium panels: the same for $\Delta T(x)$ in logarithmic scale. $B=7$ T, $T_L = 4$ K, other parameters as in Figs. 1 and 2.

the conductivity ($\lambda = 0$ in Eq. (A6) of the Appendix). We have repeated the calculation for stronger heating effects, $p=0.5$, and for two kinds of spatial averaging, $\lambda = \ell_B$ ($=9.7$ nm at $B=7$ T) and $\lambda = \lambda_F/2$ ($=23.3$ nm, corresponding to $\langle n_{el}\rangle = 2.9\cdot10^{11}$ cm^{-2}). The result is qualitatively the same, but now the discontinuities (and hysteretic behaviors) occur already for lower imposed currents, $I \gtrsim 0.55$ μA, however only at lower lattice temperature, $T_L \lesssim 2.3$ K.

The model of homogeneous positive background charge ($n_D = 4\cdot10^{11}$ cm^{-2}) considered here, yields for $B=7$ T at low temperatures near $|x| = 0.53d$ relatively wide incompressible stripes (width ~75 nm for $I=0$), so that the spatial average over λ has no drastic effect, at least not for small applied currents. This can be seen from Fig. 6, which compares averaging over the magnetic length ($\lambda = \ell_B$) with averaging over the B-independent Fermi wavelength ($\lambda = \lambda_F/2$), for two different temperatures. For comparison, also the Drude result for the Hall resistance, $R_H^D = h/(e^2\bar{\nu}_{eff})$, is shown, where $\bar{\nu}_{eff} = 2\pi\ell_B^2\langle n_{el}\rangle/0.9$ considers the effective width of the 2DES. Both, increasing the temperature and increasing the averaging length λ, shortens the QHP at the low-B side, but has only little effect on the high-B edge of the quantized Hall plateau near $B=7.35$ T. Therefore it is interesting to calculate the temperature dependence of the resistances also for magnetic fields near the low-B edge of the ($\nu = 2$)-QHP, where the λ-averaging becomes important.

Results of such a calculation for $B=6$ T, where the width of the

ISs in thermal equilibrium is only about 40 nm, are shown in Fig. 7 with consideration of Joule heating ($p=0.1$) and spatial averaging ($\lambda = \ell_B = 10.5$ nm). Comparison with the classical Drude result for the Hall resistance explains why, for small imposed currents I, the breakdown of the QHE leads now to smaller values of the Hall resistance, while for $B=7$ T it leads to larger values (see Fig. 4). If we require for the QHE $R_{long}/R_{Hall} \lesssim 10^{-4}$, we find that the QHP extends down to $B=6$ T only for low lattice temperatures, $T_L \lesssim 2.5$ K. If one fixes T_L near this value, R_{long} increases with increasing imposed current I, while R_{Hall} decreases towards the classical Drude value at that temperature (see Fig. 7 at $1/T_L \sim 0.4$ K^{-1}). Thus we observe a continuous breakdown of the QHE.

For higher imposed currents ($I \gtrsim 0.4$ μA) and lower temperature ($T_L \lesssim 1.9$ K) we find again hysteretic behavior, which is similar to that obtained for $B=7$ T (see Fig. 4), but occurs already at much smaller imposed currents (for $I \gtrsim 0.4$ μA), but only at lower temperatures ($T_L \lesssim 1.9$ K).

3.3. Comparison with experiments

3.3.1. Edge-dominated regime

In the breakdown experiments [5,15] usually the temperature is fixed while the imposed current is increased. As we see from Figs. 4 and 7, the results for longitudinal and Hall resistance
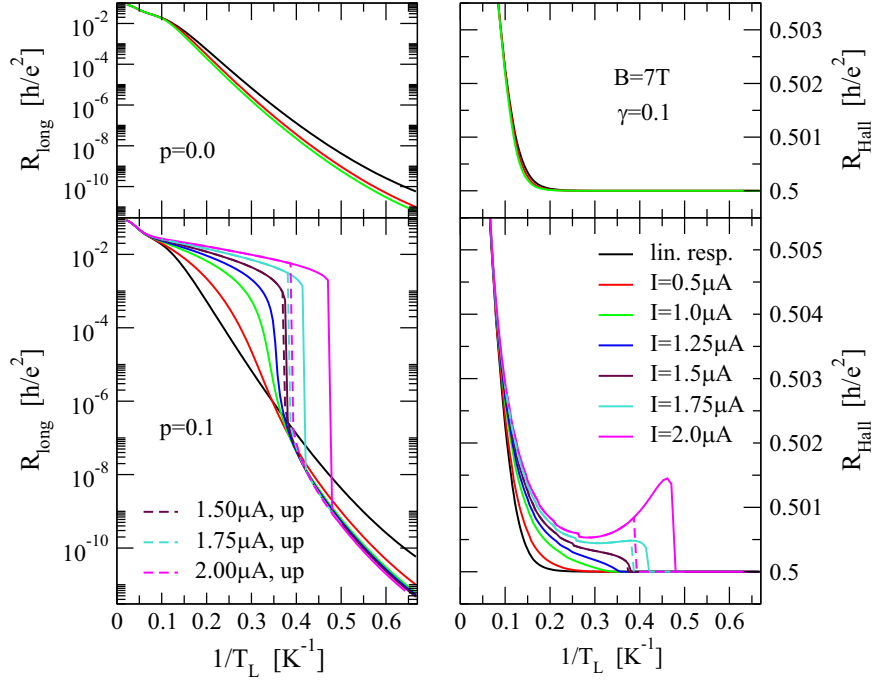
Fig. 4. Dependence of Hall resistance $R_{\text{Hall}} = [\mu^\star(d) - \mu^\star(-d)]/(eI)$ (right panels) and longitudinal resistance $R_{\text{long}} = 2d\, E_y^0/I$ (left panels) on the lattice temperature T_L, for $1.5\,\text{K} < T_L < 50\,\text{K}$, for several values of the applied current I; $N = 1000$, $\lambda = 0$, i.e. no spatial average, without (upper panels, $p = 0$) and with (lower panels, $p = 0.1$) Joule heating. In the lower panels the T_L-dependence shows a hysteresis for $I \gtrsim 1.5\,\mu\text{A}$.
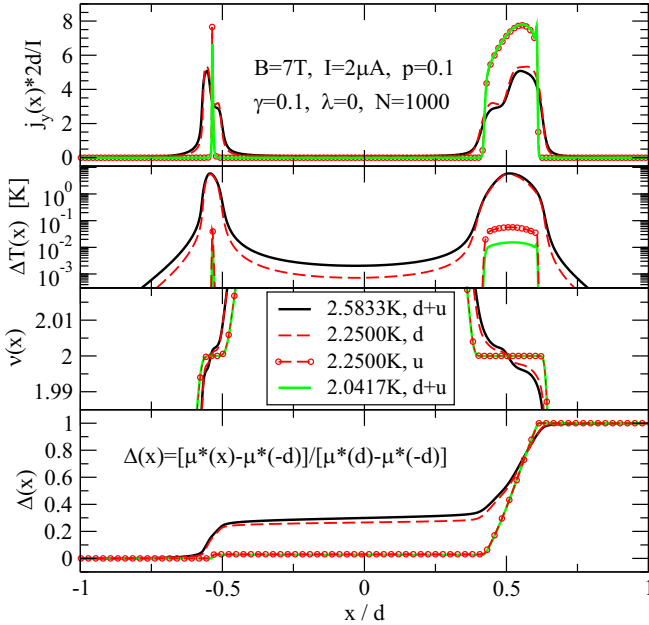

Fig. 5. Current density, increase of local electron temperature, filling factor, and normalized Hall potential for the imposed current $I = 2\,\mu\text{A}$ and states with T_L close to and in between the critical temperatures. At $T_L = 2.5833\,\text{K} \gtrsim T_{\text{cr}}^{\text{up}}(I)$ and $T_L = 2.0417\,\text{K} \lesssim T_{\text{cr}}(I)$ raising and lowering of T_L leads to the same state, but at $T_L = 2.25\,\text{K}$ in between these critical values not. States reached by lowering of T_L are labeled with 'd', those by increasing T_L with 'u'. Other parameters as in Fig. 4.

Fig. 6. Linear response result for B-dependence of Hall resistance $R_{\text{Hall}} = [\mu^\star(d) - \mu^\star(-d)]/(eI)$ (upper panel) and longitudinal resistance $R_{\text{long}} = 2d\, E_y^0/I$ in linear (central panel) and logarithmic (lower panel) scale. Results are shown for two temperatures and two choices of the spatial average length, $\lambda = \ell_B = \sqrt{10\text{T}/B}\cdot 8.1\,\text{nm}$ and $\lambda = \lambda_F/2$. Drude: $R_H^D = h/(e^2\bar\nu_{\text{eff}})$.

measured in such experiments will depend strongly on the temperature, at which the data are taken. At relatively high lattice temperatures, $T_L \gtrsim 3\,\text{K}$, the longitudinal resistance will monotonically increase with increasing current for all B-values in the ($\nu = 2$)-QHP. But if the data are taken at lower temperature, the situation may become more complicated, as is demonstrated by Fig. 8. Here the lattice temperature is taken as $T_L = 2.5\,\text{K}$ and the
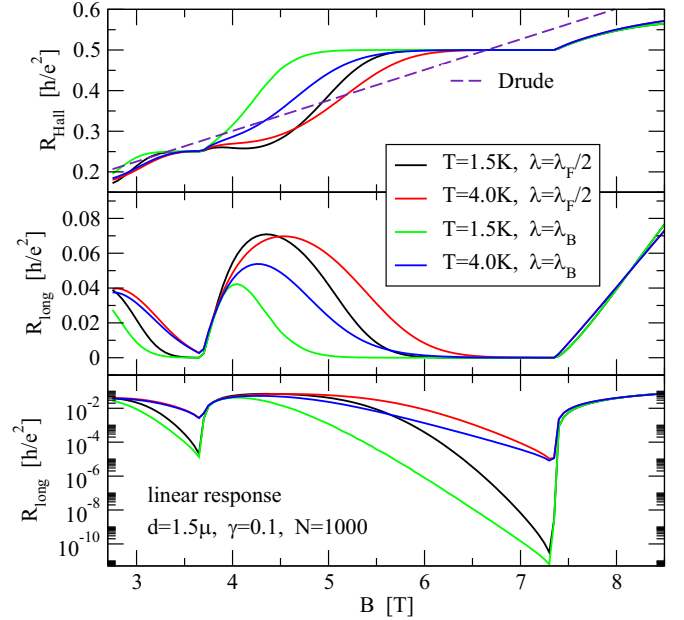
material parameters are chosen as in Fig. 7. Requiring for the IQHE $R_{\text{long}}/R_{\text{Hall}} \lesssim 10^{-4}$, we find in the linear response regime ($I \approx 0$) a ($\nu = 2$)-plateau at $6\,\text{T} \lesssim B \lesssim 7.35\,\text{T}$. The result for $B = 5.5\,\text{T}$ below the low-B edge of the plateau does not satisfy the requirement for the IQHE and that for $B = 7.4\,\text{T}$ above the high-B edge of the plateau shows essentially linear response behavior without any tendency towards the IQHE.

In the low-B part of the plateau, $6\,\text{T} \lesssim B \lesssim 6.7\,\text{T}$, we find a continuous breakdown of the IQHE. If we define a critical current
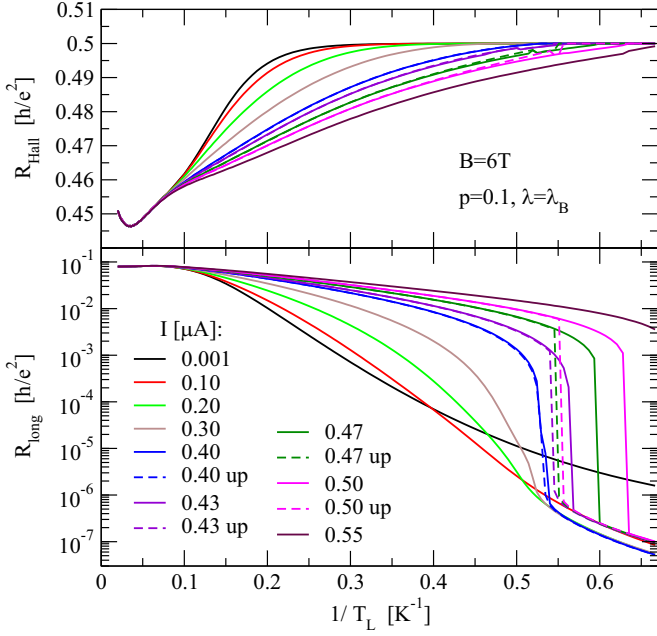
Fig. 7. Hall resistance $R_{\mathrm{Hall}} = [\mu^\star(d) - \mu^\star(-d)]/(eI)$ and longitudinal resistance $R_{\mathrm{long}} = 2d\,E_y^0/I$ versus inverse lattice temperature for $B = 6$ T and different applied currents, with Joule heating ($p=0.1$) and spatial averaging ($\lambda = \ell_B$); other parameters as in Fig. 4.
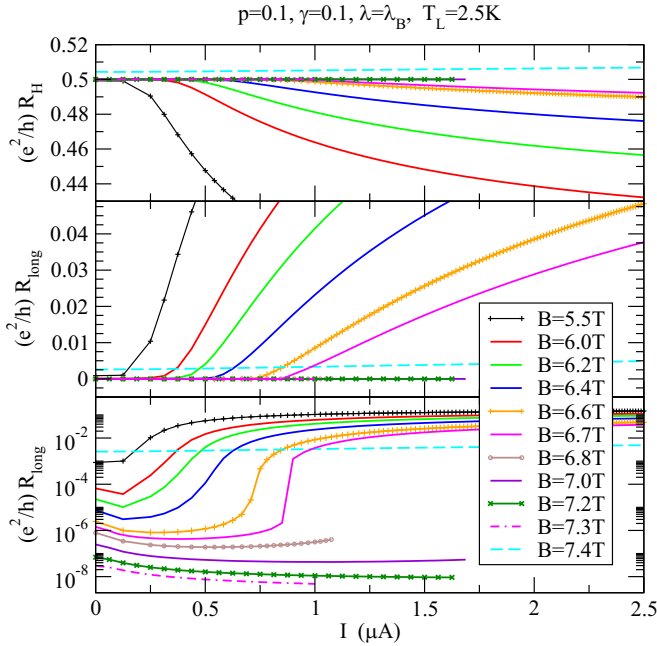

Fig. 8. Hall resistance (upper panel) and longitudinal resistance, in linear (medium) and logarithmic scale (lower panel), versus imposed current I for several B-values and $T_L = 2.5$ K, with Joule heating ($p=0.1$) and spatial averaging ($\lambda = \ell_B$); other parameters as in Fig. 4. Location of the QHP (for $I=0$): $6\,\mathrm{T} \lesssim B \lesssim 7.35\,\mathrm{T}$.

$I_{\mathrm{cr}}(B)$ as the current at which $R_{\mathrm{long}}(I)$ becomes larger than 10^{-4} h/e^2, $I_{\mathrm{cr}}(B)$ increases monotonously with increasing B. In the breakdown regime $I \gtrsim I_{\mathrm{cr}}(B)$ the slopes of the curves $R_{\mathrm{long}}(I)$ are of the same order of magnitude but decrease slightly with increasing B. All these features, shown in the middle panel of Fig. 8, are in good qualitative agreement with the experimental results shown in Fig. 3 of [5]. This type of results was denoted as "edge-dominated" behavior, since in this B-region the IQHE is dominated by ISs near the sample edges, which carry the imposed current nearly

dissipationless. (In this Fig. 3 of [5] the longitudinal voltage is plotted as function of the bias voltage, which is equivalent to our plot of the longitudinal resistance as function of the imposed current.).

3.3.2. Bulk-dominated regime

The logarithmic plot in the lower panel of Fig. 8 shows some additional details. Apparently, for small imposed currents I, R_{long} decreases with increasing I. In the low-B part of the ($\nu = 2$)-plateau, $6\,\mathrm{T} \lesssim B \lesssim 6.7\,\mathrm{T}$, $R_{\mathrm{long}}(I)$ goes through a minimum and then increases monotonously, yields a continuous breakdown of the QHE and saturates at values of the order 0.1 h/e^2. Between minimum and saturation the slopes of the $R_{\mathrm{long}}(I)$ curves become very steep with increasing B. This may indicate that for $B \gtrsim 6.8$ T a discontinuous breakdown of the IQHE takes place with increasing imposed current. Unfortunately our iterative calculation, based on the Newton-Raphson-method for the solution of non-linear integral equations, does not converge in this regime. The reason for this problem may be, that the method relies on successive small changes of the thermodynamic state of the system, whereas in the hysteretic regime abrupt, large changes may be expected. The numerical results for $B \geq 6.8$ T give, however, no indication of such an abrupt increase of the longitudinal resistance.

Aiming to clarify the situation, we repeated the calculation for different parameters: stronger Joule heating, $p=0.5$, lower temperature, $T = 1.5$ K, and more effective spatial averaging of the conductivity, $\lambda = \lambda_F/2$. Results are presented in Fig. 9. Due to the larger values of p and λ the low-B edge of the ($\nu = 2$)-plateau is shifted to $B = 6.2$ T. The characteristics of the low-B part of the plateau, here $6.2\,\mathrm{T} \lesssim B \leq 6.55\,\mathrm{T}$, are similar to those of Fig. 8 and in qualitative agreement with the experiments in the "edge-dominated regime", although the structures are more pronounced and appear at smaller values of the imposed current I. The low-B part of the plateau with a continuous breakdown of the QHE ends abruptly at $B = 6.55$ T, where a current $I \gtrsim 0.2$ µA leads to the breakdown. For $B \geq 6.56$ T no tendency towards a breakdown of the QHE is observable, and the system remains in the QH state for all I-values, for which the calculation converges.
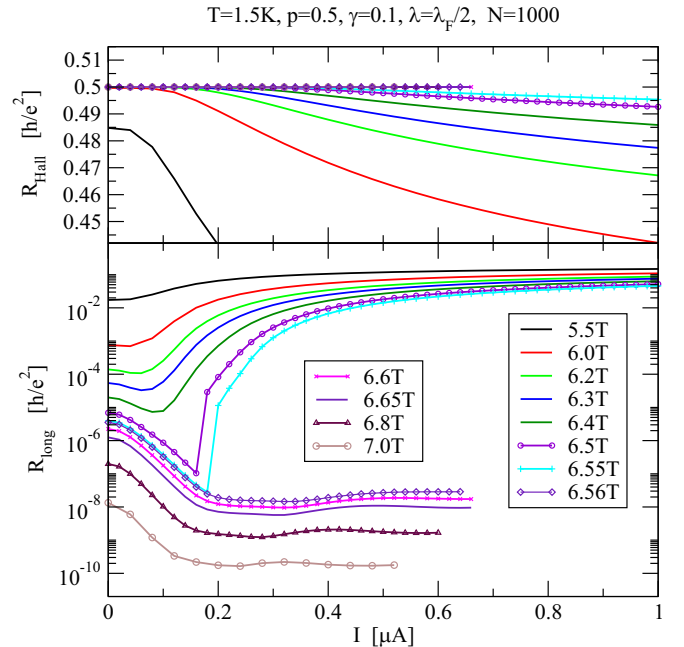

Fig. 9. Hall resistance (upper panel) and longitudinal resistance (lower panel), versus imposed current I for several B-values and $T_L = 1.5$ K, with Joule heating ($p=0.5$) and spatial averaging ($\lambda = \lambda_F/2 = 23.3$ nm); other parameters as in Fig. 4.

The results presented in Figs. 9 and 8 for the high-B part of the ($\nu = 2$)-plateau are not in agreement with the experiments, which show in this B-region a "bulk-dominated" behavior with QH states, in which the dissipationless current density is distributed over a wide part of the bulk of the sample. In this bulk-dominated region the experiments show again a continuous breakdown of the IQHE, if the imposed current (or the bias voltage) exceeds a certain B-dependent value $I_{cr}(B)$, but in contrast to the edge-dominated behavior, now $I_{cr}(B)$ decreases with increasing B, while the increase of the longitudinal voltage with increasing bias voltage (i.e. of R_{long} with increasing I) becomes steeper.

In contrast to the experimental finding in the bulk-dominated regime, our numerical results in this B-regime show no indication of a current-induced breakdown of the QHE. The reason for this discrepancy needs further investigation. Probably the present model of a homogeneous positive background charge density describing donor-doping is too simple. It leads to an electron density with a maximum in the middle of the sample and a monotonous decrease towards the edges. This leads to incompressible stripes, which, with increasing B, become broader and move towards the center of the sample. In the high-B region of the ($\nu = 2$)-plateau this leads to broad ISs, which can carry large dissipationless currents, so that Joule heating is not effective. This might require another breakdown mechanism of the IQHE. However, the experiments have shown that the electron density is not homogeneous along the sample and that fluctuations may lead to abrupt changes in the Hall potential profile at different cross sections along the sample (see Figs. 5 and A4 of [5]). Fluctuations of the electron density, enhanced by the non-linear feedback effects in strong imposed currents, may lead to inhomogeneous incompressible regions which are locally sensitive to Joule heating.

4. Summary

We have extended the previously used self-consistent screening theory of stationary magneto-transport in narrow Hall bars [6,9] by the inclusion of Joule heating and heat transfer to the lattice. The calculated results are compared with recent measurements of the local distribution of current density and Hall potential in such samples under the conditions of the IQHE and its breakdown, enforced by imposed currents at low lattice temperatures.

A nice qualitative agreement between theory and experiment is obtained in the so called "edge-dominated regime" of the IQHE, in which the imposed current I flows, nearly dissipation-less, through incompressible stripes near the sample edges. With increasing strength of I one finds an increasing asymmetry of the stripes and of the currents through and the Hall voltages across these stripes. If I increases further, the calculation yields an increasing electron temperature in the stripes, which leads to a modification of the electron density in the stripes and thus to a continuous breakdown of the IQHE. The resulting I-dependence of the longitudinal resistance shows a characteristic dependence on the magnetic field B, consistent with that found in the experiments [5].

In contrast to the experiments, in the calculations the lattice temperature T_L is easily changed, while keeping B and I fixed. Lowering T_L, one finds for sufficiently large I at a critical $T_L = T_{cr}(I)$ a discontinuous transition from a dissipative normal state to a state showing the IQHE. If T_L is lowered further, the system remains in a quantized state. If T_L is raised again, the system remains in a quantized state until it jumps back to a normal dissipative state at a temperature $T_L = T_{cr}^{up}(I) > T_{cr}(I)$. This type of hysteresis is well known for "macroscopic" samples and has been discussed in the literature [17,18]. It may be interesting to explore it experimentally at the microscopic samples considered here [5].

An apparent discrepancy between experiment and calculation is found in the high-B part of the ($\nu = 2$)-QHP, the "bulk-dominated" regime. Here the experiments yield, for low currents (or bias voltages), a distribution of the dissipation-less current and the corresponding variation of the Hall potential over a wide part of the Hall bar. At higher currents again an apparently continuous breakdown of the IQHE is observed, but now the critical currents and the slopes of the R_{long}-versus-I curves show a different dependence on B as in the edge-dominated regime. The calculations, performed at fixed $T_L \leq 2.5$ K and fixed B in the upper part of the QHP, show no current-induced breakdown of the IQHE. The reason is probably the simple model for the electron density in the 2DES, which does not allow for fluctuations. It yields wide ISs near the center of the Hall bar, which, at low T_L, can carry large currents nearly dissipation-less, so that Joule heating is not effective. Since the experiments [5] clearly demonstrate the presence and importance of density fluctuations, such fluctuations should be incorporated into the theoretical model. They may lead to spatial structures in the current-carrying incompressible regions, which are sensitive to Joule heating. These questions need further investigation.

Acknowledgments

Appendix A

As in [9] we take $D(E) = D_0 = m/(\pi\hbar^2)$ for the density of states at $B=0$, with $m = 0.067m_0$ the effective mass of GaAs, and for large, quantizing magnetic fields

$$D(E) = \frac{1}{\pi\ell_B^2}\sum_{n=0}^{\infty} A_n(E), \quad A_n(E) = \frac{1}{\sqrt{\pi}\Gamma}\exp(-[E_n - E]^2/\Gamma^2), \tag{A1}$$

with $E_n = \hbar\omega_c(n + 1/2)$ the Landau energies, $\omega_c = eB/mc$ the cyclotron frequency, and a Gaussian form of the spectral function, where the width is given by $\Gamma = \gamma\hbar\omega_c[10\ \mathrm{T}/B]^{1/2}$, with γ a measure of the collision broadening. The conductivities $\sigma_{xx}(x) = \sigma_{yy}(x) = \sigma_\ell(x)$ and $\sigma_{yx}(x) = -\sigma_{xy}(x) = \sigma_H(x)$ are given by

$$\sigma_H(x) = (e^2/h)\nu(x), \quad \nu(x) = 2\pi\ell_B^2 n_{el}(x), \tag{A2}$$

$$\sigma_\ell(x) = \frac{e^2}{h}\int_{-\infty}^{\infty} dE[-f_E'] \sum_{n=0}^{\infty} (2n + 1)[\sqrt{\pi}\Gamma A_n(E)]^2, \tag{A3}$$

where $n_{el}(x)$ is calculated according to Eq. (4) with the argument of the Fermi function replaced by $[E + V(x) - \mu^*(x)]/k_B T_{el}(x)$ and where $f_E' = \partial f([E + V(x) - \mu^*(x)]/k_B T_{el}(x))/\partial E$. From Ohm's law we obtain, with $\rho_\ell(x) = \sigma_\ell(x)/[\sigma_\ell(x)^2 + \sigma_H(x)^2]$ and $\rho_H(x) = \sigma_H(x)/[\sigma_\ell(x)^2 + \sigma_H(x)^2]$,

$$j_y(x) = E_y^0/\rho_\ell(x), \quad E_x(x) = \rho_H(x)j_y(x), \quad \int_{-d}^{d} dx j_y(x) = I, \tag{A4}$$

and

$$\mu^*(x, y) = eE_y^0 y + \mu^*(x), \quad \mu^*(x) = \mu_0^* + eE_y^0\int_0^x dx'\rho_H(x')/\rho_\ell(x'), \tag{A5}$$

so that $E_y^0 = I/\int_{-d}^{d} dx[1/\rho_\ell(x)]$. The y-dependent term $eE_y^0 y$ must also be added to $V(x)$, to ensure that $V(x, y) - \mu^*(x, y) = V(x) - \mu^*(x)$,

and as a consequence the electron density, is independent of y. The constant μ_0^* is determined by the average electron density [9]. To avoid spurious incompressible stripes of extremely small width, we again smoothen the conductivity tensor

$$\hat{\sigma}(x) = \frac{1}{2\lambda} \int_{-\lambda}^{\lambda} d\xi\, \hat{\sigma}(x + \xi). \tag{A6}$$

with a suitable length λ.

References

[1] P. Weitz, E. Ahlswede, J. Weis, K. von Klitzing, K. Eberl, Appl. Surf. Sci. 157 (2000) 349.
[2] P. Weitz, E. Ahlswede, J. Weis, K. von Klitzing, K. Eberl, Physica E 6 (2000) 247.
[3] E. Ahlswede, P. Weitz, J. Weis, K. von Klitzing, K. Eberl, Physica B 298 (2001) 562.
[4] E. Ahlswede, J. Weis, K. von Klitzing, K. Eberl, Physica E 12 (2001) 165.
[5] K. Panos, R.R. Gerhardts, J. Weis, K. von Klitzing, New J. Phys. 16 (2014) 113071.
[6] K. Güven, R.R. Gerhardts, Phys. Rev. B 67 (2003) 115327.
[7] A. Siddiki, R.R. Gerhardts, Phys. Rev. B 70 (2004) 195335.
[8] R.R. Gerhardts, Phys. Status Solidi B 245 (2008) 378.
[9] R.R. Gerhardts, K. Panos, J. Weis, New J. Phys. 15 (2013) 073034.
[10] K. von Klitzing, G. Dorda, M. Pepper, Phys. Rev. Lett. 45 (1980) 494.
[11] D.B. Chklovskii, B.I. Shklovskii, L.I. Glazman, Phys. Rev. B 46 (1992) 4026.
[12] D.B. Chklovskii, K.A. Matveev, B.I. Shklovskii, Phys. Rev. B 47 (1993) 12605.
[13] K. Lier, R.R. Gerhardts, Phys. Rev. B 50 (1994) 7757.
[14] J.H. Oh, R.R. Gerhardts, Phys. Rev. B 56 (1997) 13519.
[15] K. Panos, Ph.D. Thesis, Universität Stuttgart, 2014.
[16] S. Komiyama, T. Takamasu, S. Hiyamizu, S. Sasa, Solid State Commun. 54 (1985) 479.
[17] G. Nachtwei, Physica E 4 (1999) 79.
[18] S. Komiyama, Y. Kawaguchi, Phys. Rev. B 61 (2000) 2014.
[19] S. Kanamaru, H. Suzuura, H. Akera, J. Phys. Soc. Jpn. 75 (2006) 064701.